1   **A new technique for the detection of large scale landslides in glacio-lacustrine deposits using**

2   **image correlation based upon aerial imagery: a case study from the French Alps**

3   Paz Fernandez [1] and Malcolm Whitworth [2]

4   [1] Department of Civil Engineering, ETSICCP, University of Granada, Campus de Fuentenueva, E-
5   18071, Granada, Spain e-mail: pazferol@ugr.es

6   [2] School of Earth and Environmental Sciences, University of Portsmouth, Burnaby Road, Portsmouth
7   PO1 3QL. United Kingdom. Email: malcolm.whitworth@port.ac.uk

8   **Abstract**

9   Landslide monitoring has benefited from recent advances in the use of image correlation of high
10   resolution optical imagery. However, this approach has typically involved satellite imagery that may
11   not be available for all landslides depending on their time of movement and location. This study has
12   investigated the application of image correlation techniques applied to a sequence of aerial imagery
13   to an active landslide in the French Alps. We apply an indirect landslide monitoring technique (COSI-
14   Corr) based upon the cross-correlation between aerial photographs, to obtain horizontal
15   displacement rates. Results for the2001–2003 time interval are presented, providing a spatial model
16   of landslide activity and motion across the landslide, which is consistent with previous studies. The
17   study has identified areas of new landslide activity in addition to known areas and through image
18   decorrelation has identified and mapped two new lateral landslides within the main landslide
19   complex. This new approach for landslide monitoring is likely to be of wide applicability to other
20   areas characterised by complex ground displacements.

23

1. Introduction

Landslide monitoring is a very important part of any landslide hazard assessment, providing a measure of the rate and direction of slope movement in order to quantify any potential landslide risk. Different types of monitoring techniques can be employed, depending on the scale and frequency of observations required; they include in-situ instrumentation, but these provide movement data at a single location on the landslide; and are often difficult to install on very active landslides. Other options include remote ground based monitoring such as ground based radar (Monserrat et al., 2014), terrestrial laser scanning (Jaboyedoff et al., 2012;Delacourt et al., 2007; Teza et al., 2008) and multi-temporal terrestrial photography (Gance et al., 2014; Travelletti et al., 2012), but these require a clear line of sight in order to monitor the entire land-slide effectively. By contrast, satellite and airborne remote sensing platforms offer better visibility and coverage of the ground surface by virtue of the vertical imaging geometry. Monitoring has been performed using digital photogrammetry applied to aerial imagery (Casson et al., 2003; Fabris et al., 2011), radar interferometry (Wasowski and Bovenga, 2014) and comparison of LiDAR derive delevation models (Daehne and Corsini, 2013). More recently, image matching has been applied to aerial and satellite imagery to monitor slope movement, by comparing two remote sensing images of a landslide from different dates to identify and quantify sur-face changes. This type of image matching or image correlation approach has been applied to landslide monitoring using aerial stereo-pairs and satellite imagery in this area, like aerial stereo-pairs used in La Clapiere landslide to understand its dynamics(Booth et al., 2013; Casson et al., 2003; Delacourt et al., 2007) and LiDAR point cloud data (Travelletti et al., 2012). However, there are no examples that use aerial photography and image matching asthe basis for landslide monitoring. There may be occasions when satellite imagery or high resolution topographic data are unavailable, either due to the age of the movement or simply through a lack of data coverage. In these circumstances, the use of aerial photography can offer opportunities for landslide monitoring, whereby aerial imagery from two different dates can provide the basis for identifying and measuring landslide movement.

In this study, we present the application of an image matching technique to the study of an active glacio-lacustrine landslide in the French Alps, using aerial photography as a basis for the image correlation. This contrasts with previous studies that have principally relied upon satellite platforms to provide the imagery for the comparison. We demonstrate the suitability of COSI-Corr software (Ayoub et al., 2009), to the study of landslide movement based upon aerial photography, rather than satellite imagery or topographic data; and identify the steps, information and conditions necessary for successful application to landslide monitoring. The technique has been applied in the Harmaliere

57   landslide to firstly, identify areas of landslide activity and secondly, obtain horizontal displacement
58   rates on the active part of the landslide.

59   **1.1 Geological context and landslide study area**

60   In France, some of the largest and most problematic landslides in the Alps are associated with
61   Quaternary glacio-lacustrine deposits that infill many of the alpine valleys. These lake deposits
62   typically consist of fine grained finely laminated (varved) silts and clays deposited in dammed lakes
63   impounded by valley glaciers during previous glacial advances. The deposits have been exposed by
64   the local river network that has cut down deeply into these clay formations; consequently, in many
65   places, these deposits make up much of the slope forming materials within the valleys. The
66   geotechnical nature of these deposits is such that this exposure has resulted in significant slope
67   instability (Giraud et al. 1991; van Asch et al. 1996).

68   The Harmaliere landslide, documented in this study, is located in the Trieves region of the French
69   Alps, near the village of Sinard in the Drac valley, 40km south of Grenoble in an area of extensive
70   glacio-lacustrine deposit exposure (Fig1). Here the glacio-lacustrine deposits cover an area of 300
71   km^2 and were deposited in lakes impounded by the Isiere Glacier during the Wurm maximum
72   episode (Van Asch et al. 2009). The thickness of the laminated clays in this region varies from 0 to
73   250 metres, reflecting the uneven nature of the base of the lakes in which deposition took place. The
74   deposits have been exposed by the local river network that has cut down deeply into these clay
75   formations; consequently, in many places, including the Drac valley, these deposits make up much of
76   the slope forming materials within the valleys. The geotechnical nature of these deposits is such that
77   this exposure has resulted in significant slope instability, which poses a hazard to local population
78   centres and infrastructure (Antoine et al. 1992; Giraud et al. 1991; vanAsch et al. 1996).

79   The Harmaliere landslide underwent a major initial movement in March 1981 following a period
80   of quiescence. The main initiation event is illustrated in Fig2 and Fig3, the landslide is shown in its
81   pre-failure state on aerial imagery acquired in 1948 (Fig2), this contrasts with the second image
82   taken in 1981 (Fig3), just after the main activation, where the landslide can be seen to have
83   undergone a major retrocession and advanced down the valley into the Lac de Monteynard (this lake
84   was filled following completion of the Monteynard Dam in 1961 and so not visible in the earlier 1948
85   images). Since 1981 the landslide has retrogressed repeatedly through a number of episodic events
86   at the head of the landslide in 1988, 1996 and 2001 (Bièvre et al. 2011).
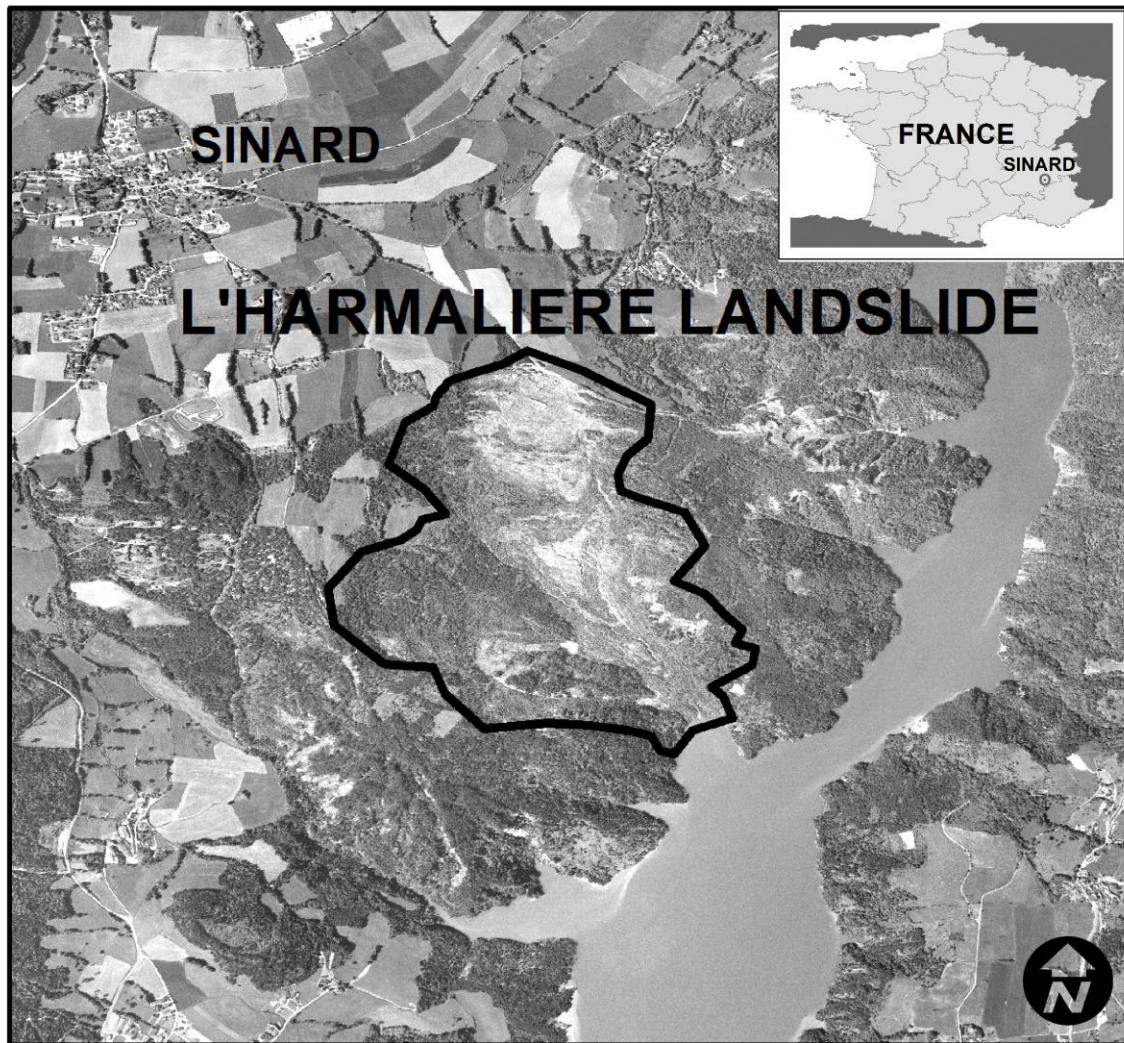
Fig1. Location and view of the Harmaliere landslide area with its outlines. It is situated near the village of Sinard, within the Drac valley 40 kilometers south of the Grenoble city, France.

In between, however the landslide has displayed evidence of mass redistribution throughout the slope and a number of lateral landslide events.

Geotechnical investigations of the neighbouring Avignonet landslide indicates that the landslide movement in this area typically involves several slip surfaces at shallow depths of 5 to 15 metres and depths of greater than 50m (Jongmans et al. 2009). Consequently, a range of slide velocities are observed, as landslides of different depths respond to climatic events, such as rain and snow melt. Bièvre et al. (2011) documented velocity variations between a few centimeters to several tens of metres per year across the Avignonet and Hermaliare slides, with a mean regression rate up to 10 metres/year measured from aerial photographic analysis (Jongmans et al. 2009; Jongmans et al.

100   2008). Importantly, relict landslides are likely to be present in this area; given the length of time river

101   erosion has been acting along the Drac valleys following glacial retreat, the river erosion and

102   downcutting during this period of associated climatic amelioration would have resulted in a long

103   period of landslide activity. Therefore, relict landslides are postulated to exist in many of the slopes

104   in this area, indeed the image take in 1948 (Fig2) provides geomorphological evidence of superficial

105   landslide activity even prior to the major event in 1981 (Fig3).

106   Geologically, the area is characterised by an undulating carbonate bedrock that is overlain by a 250

107   metre stack of Quaternary glacial, fluvial and lacustrine deposits formed at the frontal margin of a

108   valley glacier (Isere Glacier,). The superficial deposits are the result of a series of glacial and inter-

109   glacial events that have affected the Alps over the past 200k years, including Wiss glaciation (200-

110   130ky BP), Wiss-Wurm interglacial (130-100ky BP) and the most recently, the Wurm (100-12ky BP).

111   At the peak of this latest glacial period (24-18ky BP) the region was affected by the Isere Glacier,

112   which moved from the north, past Grenoble and into the Drac valley, subsequently terminating close

113   to the village of Sinard nearby the Hermaliere landslide locality. The base of the Quaternary

114   sediment sequence comprises coarse fluvio-glacial deposits that rest unconformably on the Jurassic

115   carbonate bedrock. They are dominated by extensive outwash sheets of fluvial deposits and channel

116   infill that represent the initial phase of erosion and sedimentation during the early glacial and inter-

117   glacial periods. This was then followed by the advance of the Isere and surrounding glaciers and

118   impounding of a lake, which was progressively infilled with varved glacio-lacustrine deposits. These

119   deposits typically rest conformably on the fluvial deposits (Fig4) or in some places rest directly on

120   the bedrock. The sharp contact between these two sequences (observed in Fig4) suggests a

121   relatively sudden cessation of sediment input and switch to low energy glacio-lacustrine (lake)

122   deposition. This was followed by a period during which the Isere Glacier fluctuated in extent, either

123   retreating or advancing and over-riding the glacio-lacustrine deposits. This produced a series of basal

124   till deposits that are interbedded with lacustrine deposits that reflect this period of ice fluctuation.

125

126

127

128   **Fig2.** Ortho-rectified aerial image of the Hermaliere landslide site prior to failure, the ortho-image

129   was generated using aerial photography taken in 1948.

130

131

132

Fig3. Ortho-rectified aerial image of the Hermaliere landslide site showing the results of the major
movement in March 1981. The ortho-image was generated using aerial photography taken in 1981.

135

136   With the end of this glaciation, ice retreat and the associated climatic amelioration, the river

137   network gradually re-established within the valley, cutting through the Quaternary deposits to form

138   the Drac river and the drainage network observed today. It is this sequence of events, the deposition

139   of a thick sequence of Quaternary deposits and subsequent down cutting that has generated the

140   conditions conducive to landsliding in this region.

141   Glacio-lacustrine deposits are very common in previously glaciated regions of the world, where pro-

142   glacial lakes have formed in which thick sequences of laminated silts and clays (varves) have been

143   deposited. Their geotechnical characteristics tend to lead to highly unstable behaviour (Fletcher et

144   al. 2002), particularly where these deposits have been uplifted and subsequently eroded. Landslides

145   in glacio-lacustrine deposits cause considerable ground related problems due to the highly sensitive

146   nature of the geological materials, the retrogressive nature of the resulting large scale failures and

147   the rapid conversion of this landslide material into mud flows once mobilised. The occurrence of

148   landslides associated with glacio-lacustrine deposits have been well documented in the Alpine

149   valleys of France (Jongmans et al. 2009), British Columbia in Canada (Evans 1982; Lu et al. 2000;

150   Jackson 2002), Estonia and Baltic region (Kohv et al. 2010) and the Italian Alps (Tibaldi et al. 2004). In

151   each case, the type of landsliding typically include rotational slides with mud flows developing in the

152   displaced material and the evolution characteristics typically involve significant retrogressive

153   behaviour (Geertsema et al. 2006; Marko et al. 2010). These landslides are often located in areas

154   where varved clays are cut into by river erosion, reducing support and exposing bedding planes

155   which dip down into the valleys (as a result of dip towards the centre of the previously ice-dammed

156   lakes).

Glacio-lacustrine deposits

Fluvio-glacial deposits
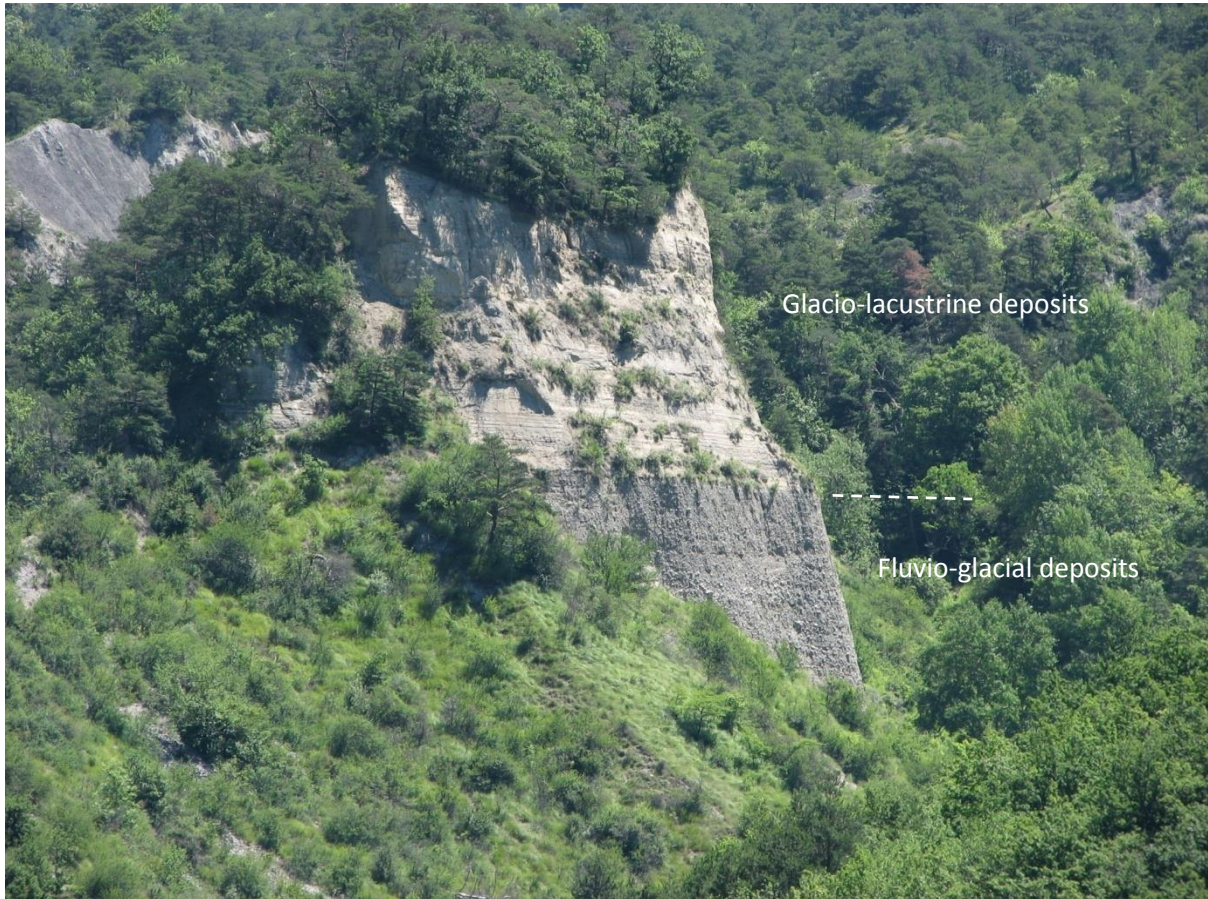
157

158 **Fig4.** Photograph showing the sharp contact between the basal coarse grained fluvio-glacial outwash
159 deposits and the overlying glacial-lacustrine deposits, illustrating the dramatic and sudden drop in
160 energy of the system from river to lake sediment deposition.

161

162

2. Data and methods

The aim of the project was to evaluate the use of image cor-relation techniques for landslide monitoring of the Harmaliere landslide using aerial photographic imagery. To this end, COSI-Corr image correlation software was used to process a sequence of aerial imagery and derive two sets of landslide displacement maps for the Hermaliere landslide. The data and methods are detailed as follows:

2.1 Image correlation techniques

Where two epochs of imagery are available for a landslide site, it is possible to compare these images manually using standard image interpretation to visually identify and map any changes that have occurred, and thereby identify areas of landslide movement. Digital image correlation, by contrast, uses statistical techniques to automatically match identical points in the two digital images and then measure their offset (in x and y) and by doing so, create a two dimensional displacement field across the landslide.

In this study, digital image correlation has been applied to a sequence of aerial photography using Cosi-Corr software (Ayoub et al. 2009; Leprince et al, 2007) in order to investigate the suitability of aerial imagery as the basis for landslide monitoring using image correlation. COSI-Corr applies Digital Image Correlation techniques using a normalised cross-correlation algorithm (NCC) to detect motions between two epochs of imagery (Le Prince et al., 2007). It has been applied successfully in several types of surface movements such as earthquakes (Copley et al. 2011; Wei et al. 2011 ; Konca et al. 2010; Barisin et al. 2009 ; Barbot et al. 2008; Leprince et al. 2008; Taylor et al. 2008; Leprince et al. 2007; Avouac et al. 2006), ice-flow (Heid and Kääb 2012; Debella-Gilo and Kääb 2011; Herman et al. 2011; Berthier et al. 2009; Quincey and Glasser 2009; Tahayt et al. 2009; Leprince et al. 2008; Scherler et al. 2008), sand migrations (Hermas et al. 2012; Necsoiu et al. 2009; Vermeesch and Drake 2008) but there are very few examples in the literature that applies this technique to landslides movements (Debella-Gilo and Kääb 2011; Leprince et al. 2008; Stumpf et al. 2014). Moreover, these COSI-Corr landslides examples use satellite images instead of aerial photographs as in our case. In each case, the image correlation has been applied to two sets of satellite imagery to create a displacement field.

2.2 Aerial imagery

The multi-temporal analysis was undertaken using 1200 dpi digitalized aerial photographs purchased from the Institut Géographique National (IGN) covering different dates, over a period covering three years, from 2001 to 2003. Consequently, RGB (3 band images: Red (R), Green (G) and Blue (B)) colour

195 aerial photographs from years 2001 and 2003 have been used in this study. These images

196 correspond to different acquisitions collected at similar altitudes and therefore scale. The flight

197 scales are between 1:23,000 and 1:25,000 approximately and flight direction was either south to

198 north and west to east (Table 1).

199 **Table 1**: Characteristics of the images used in the multi-temporal analysis

Aerial images	Date	Scale	Flight direction	Time span (days)
2001_fd0026_250_c_0267	28/05/2001	1: 23,733	S-N	783
2003_fd0038_250_c_1279	01/08/2003	1:25,830	W-E	

200

201 A combination of image pairs was chosen to minimise the temporal baselines between images in

202 order to avoid potential decorrelation between image dates. However this technique does not

203 require the use of image stereo pairs for each date, only a unique photograph that covers the entire

204 area of interest is required. There-fore the photographs were chosen where the landslide was

205 located in a more central position in the image (Table 1) (Fig. 4). How-ever the stereoscopic effect

206 could appear when we work with two images of the same area acquired from two different points of

207 view. In order to minimise stereoscopic effects low and similar incidence angles, near to vertical

208 incidence must be considered (Hermas et al.,2012; Van Puymbroeck et al., 2000). In Van

209 Puymbroeck et al. (2000) they use the parameters of the images and a DEM to model and

210 compensate the stereoscopic effect. The geometry of the shot assures an almost vertical incidence

211 angle that contributes to a negligible stereoscopic effect. Camera calibration information was

212 sourced for each of the image sets from the Institut Géographique National (IGN) and used alongside

213 the aerial photography during the initial interior orientation stage.

214 **2.2. Digital elevation model**

215 The use of a digital elevation model is not mandatory when using COSI-Corr, however, in areas of

216 high relief it is important incorporate an elevation model to correct for the topographic effects and

217 distortions during the image matching process (Ayoub et al. 2009). In this study, we use the

218 Advanced Spaceborne Thermal Emission and Reflection Radiometer (ASTER) Global Digital Elevation

219 Model ASTER GDEM V2 at 30m grid posting and acquired from USGS.

220 ASTER GDEM was released NASA and the Ministry of Economy, Trade and Industry (METI) of Japan

221 as a contribution to the Global Earth Observing System of Systems (GEOSS). ASTER GDEM (GDEM1)

222 was compiled from over 1.2 million scene-based DEMs covering land surfaces between 83°N and

223 83°Slatitudes. ASTER GDEM (GDEM2) was released by NASA and METI in mid-October, 2011

224 (Tachikawa et al. 2011). The GDEM2 has the same gridding and tile structure as GDEM1, but benefits

225 from the inclusion of 260,000 additional scenes to improve coverage, a smaller correlation kernel

226 (5x5 versus 9x9 for GDEM1) yielding higher spatial resolution, and improved water masking. The

227 absolute vertical accuracy study found the GDEM2 to be within -0.20 meters on average. (ASTER

228 GDEM V2 Validation Report, 2011).

229 2.3 Ground Control Points (GCPs)

230 GPS ground control data is required for image matching applied to aerial imagery in order to

231 perform the exterior orientation of the photographs and orientate them with reference to the

232 ground (Ayoub et al. 2009). In this study, the GPS ground control data were collected by researchers

233 at the Université Joseph Fourier, Grenoble as part of a separate research project on the Harmaliere

234 and Avignonet landslides (Bièvre et al. 2011; Jongmans et al. 2009). The GPS data was collected

235 during two different field campaigns and includes more than 40 ground control points (GCPs)

236 distributed across the entire area outside the boundary of the active landslide. The entire area

237 covers an extension bigger than the area recorded in a single image. For this reason some of the

238 GCPs were not used because they were outside the area recorded in the photographs used.

239 The campaigns were carried out with ASHTECH ProMark II devices with static acquisition method

240 with 2 seconds measurement interval and 20 minutes observation time in each point. Resulting

241 accuracy for these specifications and devices are establish in 5mm +1ppm in horizontal and 10mm

242 +2ppm in vertical coordinates.

243 Fig5 shows the GCPs distribution in 2001 photograph (left) as well as Tie points distribution over

244 2003 photograph (right).

245 2.4 Workflow

246 The processing workflow for COSI-Corr is shown in Fig6 and comprises of five stages; interior and

247 exterior orientation, ortho-rectification, resampling and final image correlation. The initial interior

248 orientation establishes the relationship between the image and camera coordinate system using the

249 fiducial marks on the image and the camera calibration report to provide a measure of the camera

250 geometry and distortions (Dewitt and Wulf, 2000). Once complete, the imagery is further

251 transformed during the exterior orientation, to real world coordinate space using GPS ground

252 control points, that provide coordinate and height information for each point located in the imagery.

253 Ayoub et al. (2009) recommend at least three ground control points per image for the exterior

254 orientation, but in this study, we used a minimum of six points per photograph (Fig5).

255

256
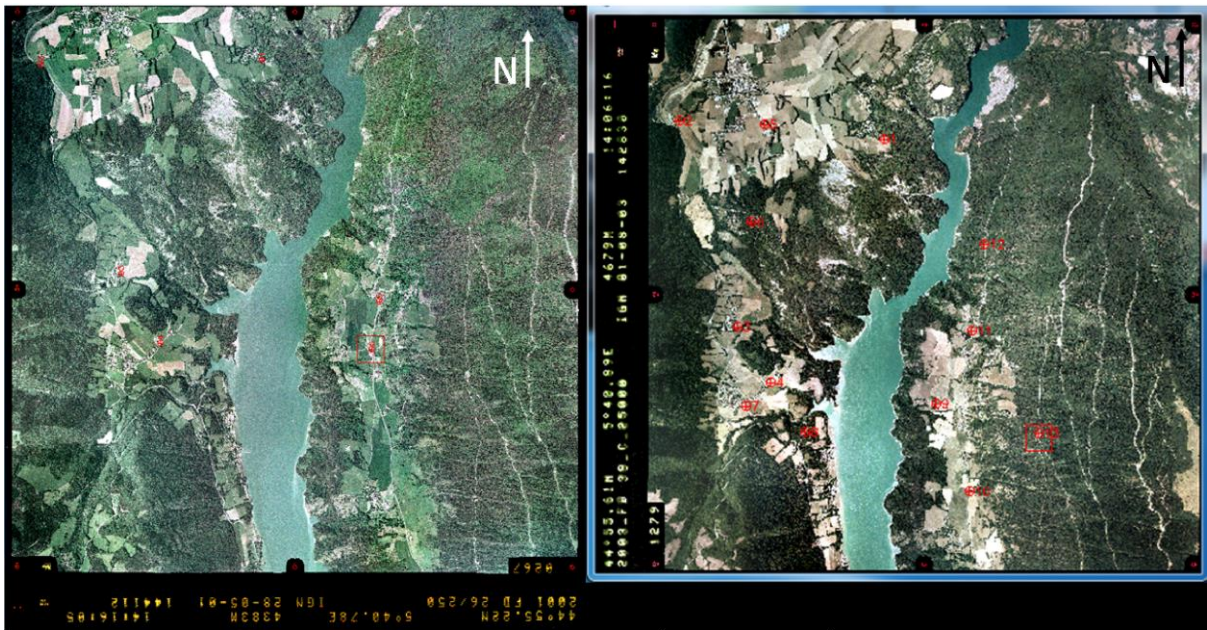
Fig5: GCPs distribution in 2001 photograph (left) as well as Tie points distribution over 2003 photograph (right).

259

260   GCP were selected from the entire list of 40 points depending on if they were clearly identified in the

261   images and their location to get a homogeneous distribution in each photograph. For the second

262   image 13 Tie points were selected by identifying homologous points manually in both images (2001

263   and 2003 photographs) to cover the entire frame surface (Fig5). The imagery was then ortho-

264   rectified using the digital elevation model and known ground control points to remove terrain

265   distortions and generate a geometrically accurate image that is then resampled to an agreed pixel

266   size and coordinate system. Concretely in this study UTM coordinate system and bilinear resampling

267   scheme were used.

268   If the aerial image comprises three RGB bands, then COSI-Corr will use only one of the bands for the

269   re-sampling process. These steps follow the traditional photogrammetric workflow applied to aerial

270   imagery (Wulf and Dewitt 2000) but applied to one image and not the standard stereopair. Once the

271   two sets of images have been generated for each data, COSI-Corr proceeds with the image

272   correlation. COSI-Corr algorithms use a Normalized Cross-Correlation (NCC) to measure the similarity

273   between matching entities in one image and their corresponding entity in a second image (Debella-

274   Gilo and Kaab 2011; Leprince et al. 2007). Once an object has been matched using its cross

275   correlation, a Euclidean offset is computed between the two images to give a displacement in x and

276   y. The resulting outputs include a West to East and North-South displacement field image and a

277   vector displacement map.

278   For the correlation step some parameters must be defined and adapted manually. In this study,

279   according with software developers' suggestion included in the COSI-Corr user´s guide (Ayoud,

280   Leprince and Keene, 2009) for noisy optical images, Statistical Correlator Engine was selected. The

281   parameters for this correlator are: window size in pixels, step in X and Y direction in pixels between

282   two sliding windows and search range in X and Y direction in pixels for the displacements. In this

283   study 10x10 pixels window size, 5 pixels step and 3 pixels search range in both X and Y directions

284   were selected.

285   **2.5 Accuracy assessment**

286   According to Leprince et al, 2007 theoretical COSI-Corr subpixel accuracy is 1/50 pixel for satellite

287   images with resolution no better than 5m. It degrades at higher resolution (because of topographic

288   roughness inducing more significant stereoscopic bias) of the order of 1/20th of the pixel size for

289   aerial photographs with metric GSD (Ayoub et al, 2009). This value corresponds to 32.5 mm

290   approximately in our research.

291
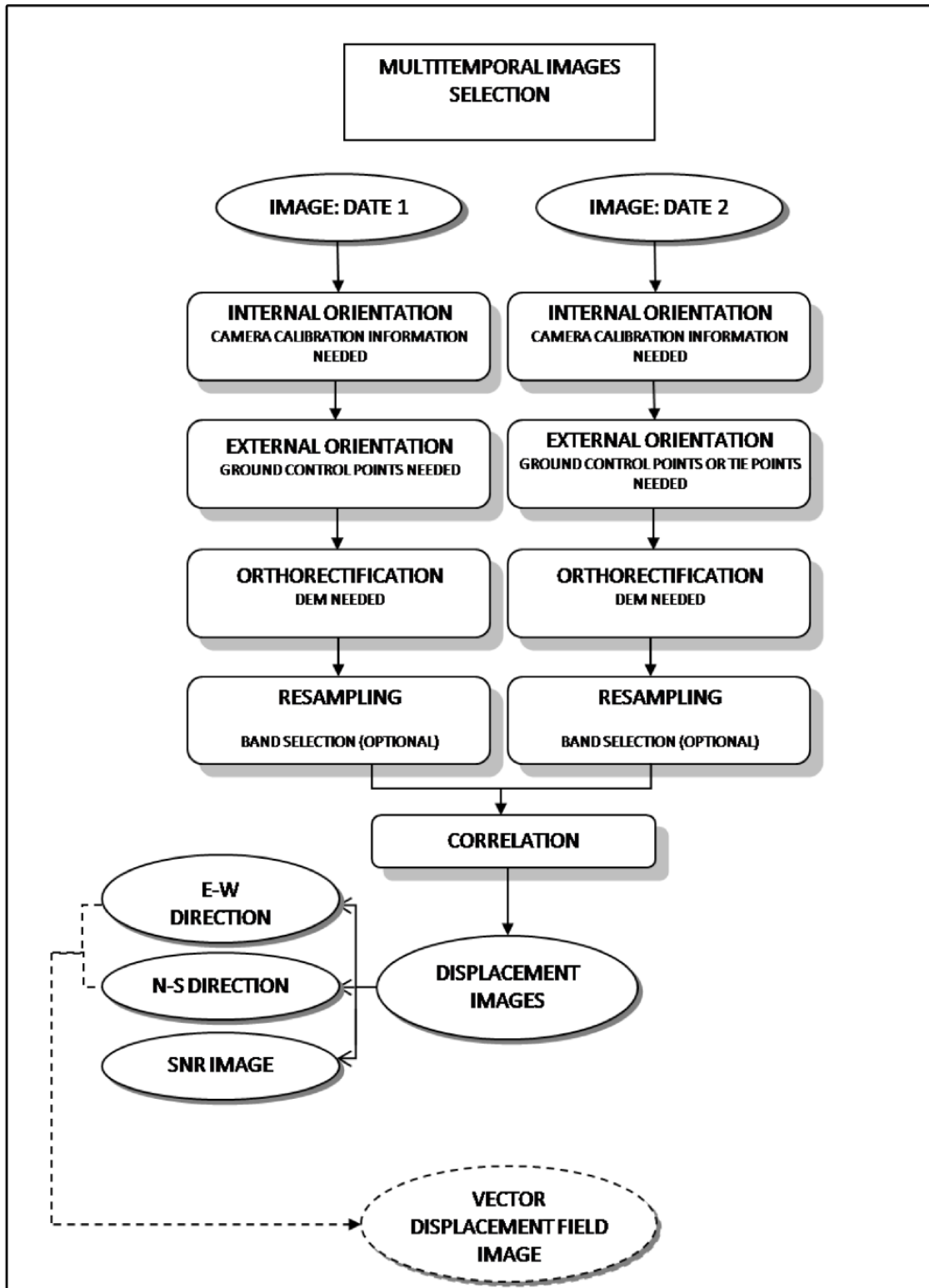
Fig6. Image matching workflow based upon aerial photographic imagery.

292

293

294

295

296 Given the activity of landslide, there are no monitoring points installed within the active parts of the
297 slide, therefore accuracy assessment of the displacement field has been assessed using prior
298 knowledge of the landslide movement (Stumpf et al. 2014), in our case, using field observations and
299 airphoto interpretation.

300 **3. Results**

301 The results of the image matching between 2001 and 2003 are shown in Fig7. The figure shows the
302 average movement direction derived from the NS and EW displacement fields. It presents areas with
303 clear slope movement, areas of decorrelation or noise have been removed. The vector field shown in
304 the figure is derived from the movement field generated from the image correlation and have been
305 added manually to the figure to provide information on the movement direction and to improve
306 clarity.

307 Zones of correlation indicate differing amounts of horizontal displacement of up to 2.5 metres.
308 There are three main zones of movement identified from the displacement field data. Firstly, a
309 strong signature of landslide motion on the western flank of the landslide is detected. The
310 differential settlement is well controlled by arcuate scarps defining a clear landslide zone in this
311 portion of the landslide complex. Some regression is visible at the top of this slope with subsidence
312 bounded by these scarps visible on the lower slopes. Localised de-correlation in this area can be
313 related to the formation of a new mudflow in this area; and this event is visible in Fig7. The eastern
314 flank also contains some displacement, particularly associated with several pre-existing lateral
315 landslides that appear to be undergoing some deformation. The major displacement is associated
316 with a second zone of decorrelation that again represents the signature of completely new
317 landslides that have formed between the two image dates (2001-2003). These new slides are clearly
318 visible in the orthoimage in Figure 8. Lastly, the head zone of the landslide contains more diffuse
319 displacement data but within this zone, some major movement in the north-west section of
320 landslide is observed moving down along the strike of the valley axis. There is evidence of some
321 displacement in the north east portion of the head zone, particularly along the major scarp zone.
322 Aerial photography does show some regression of this scarp between 2001 and 2003 and some
323 major secondary movement just downslope. The apron of landslide debris within the centre of the
324 Harmaliere valley identified by (Bievre et al. 2011) is clearly visible in the photography but shows no
325 evidence of any major displacement. Indeed, much of the landslide movement is focused at the
326 edges and back of the landslide and little movement is detected in the centre of the valley.
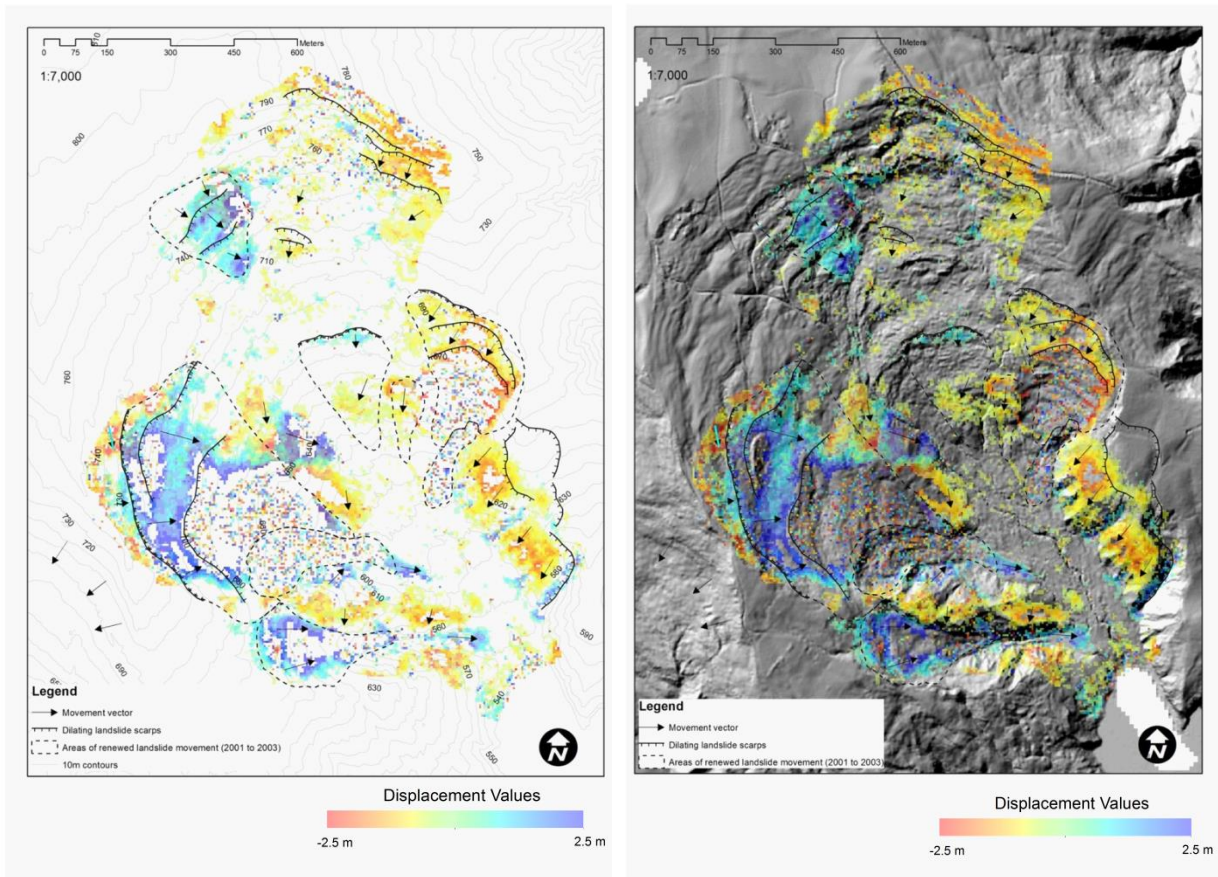
Fig7. Results of the image matching between 2001 and 2003 over contour lines (left) and DEM (right). Renewed landslide activity, scarps and slope movement vectors are shown. Displacement is cumulative over three years. Low SNR values have been mask to produce the image. Vector field displacement has been added as arrows movement direction over the image.

334   **4. Discussion**

335   The Harmaliere landslide has undergone major pulses of movement, starting in March 1981 with the
336   first major advance followed by several major retrogressive events (Bièvre et al. 2011). During the
337   intervening period, the movement is characterised smaller scale flows and lateral movements. The
338   short baseline used in this study has enabled this short temporal episodic movement to be imaged
339   alongside the major movements between 2001 and 2003. Bièvre et al. (2011) mapped temporal
340   landslide change across the Harmaliere landslide using aerial photographic interpretation for years
341   1956, 1985 and 2003. They used image thresholding to identify non-vegetated soils in the aerial
342   photography and used this to identify areas of landslide activity. Their method appears to have
343   overestimated the area of renewed activity, but despite this, for the epoch concurrent with our
344   study (2003), they detect major movement in the upper sections and west flanks of the landslide
345   which are coincident with our results. However, the displacement data isolate a number of other
346   areas of movement not identified in this previous study. Firstly, the eastern flank of the landslide is
347   much more active, with at least three new landslides detected in the displacement data. Our results
348   confirm that the western flank of the landslide in the lower part is undergoing significant movement,
349   but highlights a second landslide with a similar movement rate, not previously observed. The
350   displacement data indicates a strong component of movement for both these lateral landslides with
351   displacements of up to 2.5 metres for the period 2001 – 2003.

352   These results from our investigation suggest that the flanks of the Harmaliere landslide are
353   undergoing some deformation and that this has important implications for future landslide
354   behaviour. The lateral slope movements contribute significant material and debris into the main
355   landslide in the Harmaliere valley. This is important when considering the geomorphological setting
356   of the landslide; it is situated within a small catchment that funnels surface water down through the
357   centre of the valley and into the main Drac valley. Surface runoff is therefore concentrated in the
358   central axis of the Harmaliere valley and mobilises landslide debris that has accumulated at the
359   bottom of the valley from these lateral landslide events. This helps to explain the flow style landslide
360   behaviour that is observed in the lower part of the landslide system. The future behaviour of this
361   lower part of the landslide may therefore be linked to the process of sediment input from lateral
362   landslides, saturation and mobilisation of this debris, leading to re-activation of the lower portion of
363   the landslide and ultimately the continued regression of the upper section and head of the landslide.
364   Additionally, the head zone of the landslide is also affected by displacement, particularly the eastern
365   side of the scarp. This is also coincident with results from previous studies, which suggest that the
366   axis of the Harmaliere landslide has shifted eastward and that this is an area of increased landslide
367   movement (Bievre et al. 2011). Two major flank failures have been imaged in the displacement data.

368 Two areas of de-correlation on the east and west flanks of the landslide can be observed in the
369 displacement data and using image interpretation it is clear that these are associated with
370 completely new landslide events (see Fig7). The de-correlation stems from the mis-match between
371 the two images as a consequence of the appearance of new landslides that cannot be correlated
372 between the images. Consequently, localised de-correlation should be not dismissed but, as in this
373 case, may indicate the presence of new landslide activity.

374 Overall, the displacement data has helped us understand the behaviour of the landslide and identify
375 particular areas of renewed activity. While we recognise that the rates of movement indicated by
376 the displacement data for the period 2001-2003 cannot be validated (no GPS points are located in
377 the Harmaliere valley), the overall motion of the landslide and areas of activity revealed by the
378 image correlation are consistent with previous studies and qualitative observations from field
379 reconnaissance and aerial photographic interpretation.

380 Within the measured zone, some regions are characterised by noise caused by decorrelation
381 between the two images. These are caused by changes in surface cover, such as vegetation growth
382 or areas of new slope movement that has occurred between the dates of the two images. The
383 image analysis relies upon imagery that are free from shadow, snow and clouds so that the surface
384 topography is fully visible in both images. In this study, images were taken in May 2001 and August
385 2003 respectively at 14:10 local time (Fig. 4) in order to minimise the presence of these limiting
386 factors in the imagery.

387
388 **5. Conclusions**

389 This study has demonstrated the application of image cross-correlation to the study of landslide
390 movement using aerial photographs for the first time. The analysis has provided important insights
391 into the dynamics of the Harmaliere landslide between 2001 and 2003, and through this, we have
392 been able to identify new movement and slope deformation not previously identified or quantified.
393 The short temporal baseline has been shown to be not only a requirement for the successful
394 implementation of COSI-Corr technique for landslide monitoring; but also an advantage, in allowing
395 us to detect multi-temporal variations in the landslide movement that would have been invisible in
396 longer baseline image sets.

397 Analysing landslide movement using aerial photography and image correlation techniques we have
398 demonstrated that such monitoring is possible using aerial imagery, where high quality photography
399 and ground control data are available. This new approach for landslide monitoring is likely to be of

wide applicability to other areas characterised by complex ground displacements where aerial photographs are available for a long temporal span. In this sense aerial photographs constitute an important source of information that could be use to this purpose not only by visual image interpretation but for automatic image correlation.

Acknowledgements

References

Antoine, P., Monnet, J., Rain, N., Moulin, C. and Meriaux, P. (1992) Results of a 5 year monitoring project in the glacio-lacustrine varved clays of Trieves (southeastern France). In Bell, D. H. (ed.) 1992 Landslides: Proceedings of the Sixth International Symposium on Landslides, Christchurch, New Zealand, 10 – 14 February 1992. 1101 – 1107.

ASTER Global Digital Elevation Model Version 2 –Summary of Validation Results. August 31, 2011. http://www.jspacesystems.or.jp/ersdac/GDEM/ver2Validation/Summary_GDEM2_validation_report _final.pdf

Avouac, J. P., Ayoub, F., Leprince, S., Konca, O. and Helmberger, D. (2006). The 2005, Mw 7.6 Kashmir earthquake,rupture kinematics from sub-pixel correlation of ASTER images and seismic waveforms analysis. *Earth and Planetary Science Letters*, 249, no. 3-4, pp. 514-528.

Ayoub, F., Leprince, S., & Avouac, J.P. (2009). Co-registration and correlation of aerial photographs for ground deformation measurements. *Isprs Journal of Photogrammetry and Remote Sensing, 64*, 551-560

Ayoud, F., Leprince, S. & Keene, L. (2009). User´s Guide to COSI-CORR Co- registration of Optically Sensed Images and Correlation. California _Institute of Technology. http://www.tectonics.caltech.edu/slip_history/spot_coseis/pdf_files/cosi-corr_guide.pdf.

Barisin, I., Leprince, S. , Parsons, B.and Wright, T. (2009). Surface displacements in the September 2005 Afar rifting event from satellite image matching: Asymmetric uplift and faulting**.** *Geophys. Res. Lett.*, 36, L07301, doi:10.1029/2008GL036431.

Barbot, S., Hamiel, Y. and Fialko, Y. (2008). Space geodetic investigation of the coseismic and postseismic deformation due to the 2003 Mw7.2 Altai earthquake: Implications for the local lithospheric rheology. *Journal of Geophysical Research*, 113, B03403, doi:10.1029/2007JB005063.

Berthier, E., Le Bris, R., Mabileau, L., Testut, L., and Rémy, F. (2009). Ice wastage on the Kerguelen Islands (49°S, 69°E) between 1963 and 2006*, Journal of Geophysical Research*, 114, F03005, doi: 10.1029/2008JF001192.

Bievre, G., Kniess, U., Jongmans, D., Pathier, E., Schwartz, S., van Westen, C.J., Villemin, T., & Zumbo, V. (2011). Paleotopographic control of landslides in lacustrine deposits (Trieves plateau, French western Alps). *Geomorphology, 125*, 214-224

439 Bièvre, G., Kniess, U., Jongmans, D., Pathier, E., Schwartz, S., Van Westen, C.J., Villemin, T., & Zumbo,
440 V. (2011). Paleotopographic control of landslides in lacustrine deposits (Trièves plateau, French
441 western Alps). *Geomorphology, 125*, 214-224

442 Copley, A., Avouac, J.P., Hollingsworth, J. and Leprince, S. (2011). The 2001 M(w) 7.6 Bhuj
443 earthquake, low fault friction, and the crustal support of plate driving forces in India. J*ournal of
444 Geophysical Research - Solid Earth*, 116, Article Number: B08405, DOI: 10.1029/2010JB008137.

445 Casson, B., Delacourt, C., Baratoux, D., & Allemand, P. (2003). Seventeen years of the "La Clapiere"
446 landslide evolution analysed from ortho-rectified aerial photographs. *Engineering Geology, 68*, 123-
447 139

448 Daehne, A., & Corsini, A. (2013). Kinematics of active earthflows revealed by digital image
449 correlation and DEM subtraction techniques applied to multi-temporal LiDAR data. *Earth Surface
450 Processes and Landforms, 38*, 640-654

451 Debella-Gilo, M., & Kaab, A. (2011). Sub-pixel precision image matching for measuring surface
452 displacements on mass movements using normalized cross-correlation. *Remote Sensing of
453 Environment, 115*, 130-142

454 Delacourt, C., Allemand, P., Berthier, E., Raucoules, D., Casson, B., Grandjean, P., Pambrun, C., &
455 Varel, E. (2007). Remote-sensing techniques for analysing landslide kinematics: a review. *Bulletin de
456 la Societe Geologique de France, 178*, 89-100

457 DeWitt, B. A., & Wolf, P. R. (2000). Elements of Photogrammetry (with Applications in GIS). McGraw-
458 Hill 608 pp

459 Evans, S.G. (1982). Landslides and surficial deposits in urban areas of British Columbia: A review.
460 *Canadian Geotechnical Journal, 19*, 269-288

461 Fabris, M., Menin, A., & Achilli, V. (2011). Landslide displacement estimation by archival digital
462 photogrammetry. *Italian Journal of Remote Sensing-Rivista Italiana Di Telerilevamento, 43*, 23-30

463 Fletcher, L., Hungr, O., & Evans, S.G. (2002). Contrasting failure behaviour of two large landslides in
464 clay and silt. *Canadian Geotechnical Journal, 39*, 46-62

465 Gance, J., Malet, J.-P., Dewez, T., & Travelletti, J. (2014). Target Detection and Tracking of moving
466 objects for characterizing landslide displacements from time-lapse terrestrial optical images.
467 *Engineering Geology, 172*, 26-40

468 Geertsema, M., Clague, J. J., Schwab, J. W., & Evans, S. G. (2006). An overview of recent large
469 catastrophic landslides in northern British Columbia, Canada. Engineering Geology, 83(1), 120-143.

470 Giraud, A., Antoine, P., Van Asch, T. and Nieuwenhuisc, J. (1991) Geotechnical problems caused by
471 glaciolacustrine clays in the French Alps. Engineering Geology 31(2) 185-195.

472 Herman, F., Anderson, B. and Leprince, S. (2011). Mountain glacier velocity variation during a retreat
473 advance cycle quantified using sub pixel analysis of ASTER images. *Journal of Glaciology*, 57, Issue
474 202, pp 197-207.

475 Hermas, E., Leprince, S. and El-Magd, I.A. (2012) .Retrieving sand dune movements using sub-pixel
476 correlation of multi-temporal optical remote sensing imagery, northwest Sinai Peninsula, Egypt.
477 *Remote Sensing of Environment* 121, pp51–60

478 Heid, T. and Kääb, A.(2012). Evaluation of existing image matching methods for deriving glacier
479 surface displacements globally from optical satellite imagery. *Remote Sensing of Environment*. 118
480 pp. 339–355

481 Jackson, L.E. (2002). Landslides and landscape evolution in the Rocky Mountains and adjacent
482 Foothills area, southwestern Alberta, Canada. *Catastrophic landslides: effects, occurrence, and
483 mechanisms, Geol. Soc. Am. Rev. Eng. Geol, 15*, 325-344

484 Jongmans, D., Bièvre, G., Renalier, F., Schwartz, S., Beaurez, N., & Orengo, Y. (2009). Geophysical
485 investigation of a large landslide in glaciolacustrine clays in the Trièves area (French Alps).
486 *Engineering Geology, 109*, 45-56

Jongmans, D., Renalier, F., Kniess, U., Schwartz, S., Pathier, E., Orengo, Y., Bievre, G., Villemin, T., & Delacourt, C. (2008). Characterization of the Avignonet landslide (French Alps) with seismic techniques. *Landslides and Engineered Slopes: From the Past to the Future, Vols 1 and 2*, 395-401

Kohv, M., Talviste, P., Hang, T., & Kalm, V. (2010). Retrogressive slope failure in glaciolacustrine clays: Sauga landslide, western Estonia. *Geomorphology, 124*, 229-237

Konca, A.O., Leprince, S., Avouac, JP. and Helmberger, D. V. (2010). Rupture process of the 1999 Mw 7.1 Duzce earthquake from joint analysis of SPOT, GPS, InSAR, strong-motion, and teleseismic data: a supershear rupture with Variable Rupture Velocity. *Bulletin of the Seismological Society of America, 100, no. 1, 267-288.* doi: 10.1785/0120090072

Leprince, S., Barbot, S., Ayoub, F., & Avouac, J.P. (2007). Automatic and precise orthorectification, coregistration, and subpixel correlation of satellite images, application to ground deformation measurements. *Geoscience and Remote Sensing, IEEE Transactions on, 45*, 1529-1558

Leprince, S. , Berthier, E. Ayoub, F. Delacourt, C. and Avouac J.P. (2008). Monitoring Earth Surface Dynamics With Optical Imagery. *EOS Transactions of the American Geophysical Union*. 89, nº1. 1-2.

Marko, K., Tiit, H., Peeter, T., & Volli, K. (2010). Analysis of a retrogressive landslide in glaciolacustrine varved clay. *Engineering Geology, 116*, 109-116

Monserrat, O., Crosetto, M., & Luzi, G. (2014). A review of ground-based SAR interferometry for deformation measurement. *Isprs Journal of Photogrammetry and Remote Sensing, 93*, 40-48

Necsoiu, M., Leprince, S., Hooper, D. M., Dinwiddie, C. L., McGinnis, R. N. and Walter, G. R. (2009). Monitoring migration rates of an active subarctic dune field using optical imagery. *Remote Sensing of Environment*. 113, Issue 11, pp 2441-2447.

Quincey, D.J. and. Glasser, N.F, (2009). Morphological and ice-dynamical changes on the Tasman Glacier, New Zealand, 1990-2007, *Global and Planetary Change*, 68, Issue 3, pp. 185-197.

Scherler, D., Bookhagen, B. and Strecker, M. R. (2008). Spatially variable response of Himalayan glaciers to climate change affected by debris cover. *Nature Geoscience.* doi:10.1038/ngeo1068, 2011/01/23

Stumpf, A., Malet, J.-P., Allemand, P., & Ulrich, P. (2014). Surface reconstruction and landslide displacement measurements with Pléiades satellite images. *Isprs Journal of Photogrammetry and Remote Sensing, 95*, 1-12

Tachikawa, T., Hato, M., Kaku, M. and Iwasaki, A. 2011, The characteristics of ASTER GDEM version 2, IGARSS, July 2011.

Tahayt, A., Feigl, K.L., Mourabit, T., Rigo, A., Reilinger, R., McClusky, S., Fadil, A., Berthier E., Dorbath, L., Serroukh, M., Gomez, F., and Ben Sari, D. (2009). The Al Hoceima (Morocco) earthquake of 24 February 2004, analysis and interpretation of data from ENVISAT ASAR and SPOT5 validated by ground-based observations. *Remote Sensing Environ.*, 113(2), pp.306-316, doi: 10.1016/j.rse.2008.09.015,

Taylor, M., Leprince, S., Avouac, J.P., and Sieh, K. (2008). Detecting Co-seismic Displacements in Glaciated Regions: An Example from the Great November 2002 Denali Earthquake Using SPOT Horizontal Offsets. *Earth and Planetary Science Letters*, 270, Issues 3-4, pp. 209-220.

Teza, G., Pesci, A., Genevois, R., & Galgaro, A. (2008). Characterization of landslide ground surface kinematics from terrestrial laser scanning and strain field computation. *Geomorphology, 97*, 424-437

Tibaldi, A., Rovida, A., & Corazzato, C. (2004). A giant deep-seated slope deformation in the Italian Alps studied by paleoseismological and morphometric techniques. *Geomorphology, 58*, 27-47

Travelletti, J., Delacourt, C., Allemand, P., Malet, J.P., Schmittbuhl, J., Toussaint, R., & Bastard, M. (2012). Correlation of multi-temporal ground-based optical images for landslide monitoring: Application, potential and limitations. *Isprs Journal of Photogrammetry and Remote Sensing, 70*, 39-55

Van Asch, T.W., Malet, J., & Bogaard, T. (2009). The effect of groundwater fluctuations on the velocity pattern of slow-moving landslides. *Nat Hazards Earth Syst Sci, 9*, 739-749

Vermeesch, P. and Drake, N. (2008). Remotely sensed dune celerity and sand flux measurements of the world's fastest barchans (Bodele, Chad). *Geophys. Res. Lett.*, 35, L24404. doi:10.1029/2008GL035921,

539   Wasowski, J., & Bovenga, F. (2014). Investigating landslides and unstable slopes with satellite multi

540   temporal interferometry: current issues and future perspectives. *Engineering Geology, 174*, 103-138.

541   Wei, S., Fielding, E., Leprince, S., Sladen, A., Avouac, J.P., Helmberger, D., Hauksson, E., Chu, R.,

542   Simons, M., Hudnut, K., Herring, T. and Briggs, R. (2011). Superficial simplicity of the 2010 El Mayor–

543   Cucapah earthquake of Baja California in Mexico. *Nature Geoscience*, 4, Issue 9, 615-618, DOI:

544   10.1038/ngeo1213.